Published in final edited form as:
Front Environ Sci Eng. 2018 ; 13(1): . doi:10.1007/s11783-019-1087-6.

Source Attribution for Mercury Deposition with an Updated Atmospheric Mercury Emission Inventory in the Pearl River Delta Region, China

Jiajun Liu[a], **Long Wang**[a], **Yun Zhu**[a], **Che-Jen Lin**[b], **Carey Jang**[c], **Shuxiao Wang**[d], **Jia Xing**[d], **Bin Yu**[e], **Hui Xu**[a], **Yuzhou Pan**[a]

[a]Guangdong Provincial Key Laboratory of Atmospheric Environment and Pollution Control, College of Environment and Energy, South China University of Technology, Guangzhou Higher Education Mega Center, Guangzhou 510006, China

[b]Department of Civil and Environmental Engineering, Lamar University, Beaumont, Texas 77710, USA

[c]US EPA, Office of Air Quality Planning & Standards, Res Triangle Park, NC 27711 USA

[d]State Key Joint Laboratory of Environment Simulation and Pollution Control, School of Environment, Tsinghua University, Beijing 100084, China

[e]Guangzhou Environmental Monitoring Centre, Guangzhou, 51000, China

Abstract

We used CMAQ-Hg to simulate mercury pollution and identify main sources in the Pearl River Delta (PRD) with updated local emission inventory and latest regional and global emissions. The total anthropogenic mercury emissions in the PRD for 2014 were 11,939.6 kg. Power plants and industrial boilers were dominant sectors, responsible for 29.4 and 22.7%. We first compared model predictions and observations and the results showed a good performance. Then five scenarios with power plants (PP), municipal solid waste incineration (MSWI), industrial point sources (IP), natural sources (NAT), and boundary conditions (BCs) zeroed out separately were simulated and compared with the base case. BCs was responsible for over 30% of annual average mercury concentration and total deposition while NAT contributed around 15%. Among the anthropogenic sources, IP (22.9%) was dominant with a contribution over 20.0% and PP (18.9%) and MSWI (11.2%) ranked second and third. Results also showed that power plants were the most important emission sources in the central PRD, where the ultra-low emission for thermal power units need to be strengthened. In the northern and western PRD, cement and metal productions were priorities for mercury control. The fast growth of municipal solid waste incineration were also a key factor in the core areas. In addition, a coordinated regional mercury emission control was important for effectively controlling pollution. In the future, mercury emissions will decrease as control measures are strengthened, more attention should be paid to mercury deposition around the large point sources as high levels of pollution are observed.

Correspondence to: Long Wang (wanglong@scut.edu.cn), Yun Zhu (zhuyun@scut.edu.cn).

Keywords

Emission inventory; Mercury deposition; Pearl River Delta (PRD); Source attribution; Control strategy

1 Introduction

Mercury (Hg) is a toxic contaminant that can be bio-accumulated, and is subject to long-range atmospheric transport (Zhao et al., 2015). Once Hg is released into the atmosphere, the deposited mercury can be readily converted to methyl mercury and then accumulated in the human body or wildlife through food chain (Holmes et al., 2009). Atmospheric mercury is classified into three operationally defined species including gaseous elemental mercury (GEM or Hg^0), gaseous oxidized mercury (GOM or Hg^{2+}) and particle-bound mercury (PBM or Hg^p) (Zhang et al., 2015). GEM is the most abundant form of Hg in the atmosphere which consists of >90.0% of total gaseous mercury and has a long atmospheric lifetime of 0.5–2.0 years. GOM and PBM will deposit more rapidly downwind of their emission sources via wet or dry deposition since they have significantly higher reactivity, deposition velocities, and water solubility (Wang et al., 2014). Therefore, the chemical form of mercury has a significant effect on the spatial distribution of concentration and deposition of atmospheric mercury. In general, the pathways of anthropogenic mercury deposition vary considerably depending upon location, climate, and anthropogenic sources such as: coal combustion, nonferrous smelters, waste incineration and mining etc. (Sakata and Marumoto, 2005; Zhang et al., 2012).

China has ever been considered as the world's strongest source region of anthropogenic Hg emission because of the rapid economic and industrial growth along with a coal-dominated energy structure (Streets et al., 2005; Liang et al., 2013; Wu et al., 2016). On January 1, 2012, Ministry of Environment Protection of the People's Republic of China (MEPC) implemented the first-ever national standards for mercury from power plants named Emission standard of air pollutants for thermal power plants (GB 13223–2011). The new rules require power plants mercury emission limit to $0.03 mg/m^3$. As a matter of fact, the thermal power plants flue gas purification device has a strong mercury removal efficiency which can reach 70.0% to 85.0% after the synergistic control of electrostatic precipitation, desulphurization, denitrification (Hu and Cheng, 2016; Wang and Luo, 2017). Since then, the releases of Hg from coal-burning and nonferrous smelters have been drastically reduced in China (Zhang et al., 2015; Wu et al., 2016), but some new sources such as waste incineration, have been kept increasing which was reported more readily to deposit near the sources (Chen et al., 2013; Zhu et al., 2014). Therefore, quantifying the contribution of various emission sources to mercury deposition is essential to understand the benefits of the emission reduction efforts in China.

Previous publications provided two main methods to achieve source apportionment analysis including the Eulerian chemical transport models and receptor models (Keeler et al., 2006; Wang et al., 2015). For regional analysis, chemical transport models are preferred because receptor models are typically designed to track nearby source signals (Lin et al., 2012). In

previous studies, the contribution from selected mercury emission sources were estimated in the United States (Selin and Jacob, 2008; Lin et al., 2012) and the Great Lakes Region (Holloway et al., 2012). In China, most of the reported studies focused on mercury mass outflow and its contribution to long-distance transport pollution (Zhao et al., 2015). For the PRD, Chen et al. (2013) estimated mercury emissions from major sources and Huang et al. (2016) evaluated the impact of atmospheric mercury deposition on the environment. However, there were only a few studies relating to quantitative assessments of the contributions of mercury emission sources. Wang et al. (2014) and Zhu et al. (2015) have used different air quality models to analyse source attribution of atmospheric mercury pollution in mainland China and eastern China, respectively, the mercury pollution and source identification in specified developed regions with a high-resolution mercury inventory was seldom quantified in China.

In this paper, we firstly updated the inventory of anthropogenic atmospheric mercury in Pearl River Delta (PRD), China to 2014; and then used the Community Multiscale model (CMAQ v5.0.1) to simulate and identify sources of mercury pollution in PRD. With an understanding of temporal and spatial distribution of mercury emission, mercury concentration and deposition and contribution of main sources in the study domain, we can provide a practical mercury control pathway to mitigate mercury pollution in core areas of the PRD region effectively.

2 Methods

2.1 Emission inventory update

2.1.1 Study domain—The study domains with annual total Hg emission were presented in Fig. 1. Two nested domains were used for the CMAQ-Hg model and WRF model. The first domain (D01) covers most of China and some other parts of Asia with 175×124 horizontal grid cells at a spatial resolution of 27 km×27 km. The initial and boundary conditions (IC/BC) for D01 were extracted from GEOS-Chem global simulation results. The nested domain (D02) covers the Pearl River Delta (PRD) region, which is the focus of this study. The domain is specified between 21.491°N and 24.562°N latitudes, and 111.246°E and 115.513°E longitudes. Using the Lambert conformal projection centred at 30°N and 112°E, this domain contains 112×148 grid cells with 3 km×3 km spatial resolution and covers nine major cities (Guangzhou, Shenzhen, etc.) in Guangdong province, China. The WRF model domain was added three lines up and down and three columns left and right on the basis of CMAQ-Hg domain.

2.1.2 Mercury emission source category and estimation—The mercury emission inventory includes natural and anthropogenic sources. Natural sources mercury emissions were estimated by applying release fluxes of specific surfaces to their areas. In this paper, the bidirectional Hg exchange module in CMAQ is used to replace the previous estimates of natural and recycled Hg emissions (Bullock et al., 2008, 2009). The bidirectional surface exchange of mercury assumes that the evasion of semi-volatile pollutants deposited or produced in land surface media follow Fick’s law (Wesely and Hicks, 2000). Near-surface concentration is parameterized as a weighted average of the exchange coefficients and fluxes

at the atmospheric, cuticular, stomatal, and soil interfaces (Sutton et al., 1998). Setting bidirectional Hg in CMAQ model will only require a modified anthropogenic mercury emission inventory, other emission species should remain the same. Hg concentration and deposition fields will increase if CMAQ with bidirectional Hg exchange is run with an emissions inventory with off line estimates of natural and recycled Hg emissions. Anthropogenic mercury emissions were classified into four source categories in the inventory: (1) emission from power plants (PP), (2) emission from municipal solid waste incineration (MSWI), (3) emission from industrial point sources including industrial boilers, cement plant and metal production (IP), and (4) emission from non-industrial anthropogenic sources including on-road mobile sources, residential boilers and biomass incineration (NI).

In this study, the anthropogenic mercury emission was estimated using a bottom-up approach of Wu (Wu et al., 2016) and Zheng (Zheng et al., 2011), which needing emission factors and activity of important sectors. Formula (1) showed the equation. Activity data including energy consumption, product yields of iron, non-ferrous metals was acquired from Guangdong Statistical yearbook and Guangdong provincial pollutant statistical reports of 2014. For emissions from power plants and non-ferrous smelters which has been thoroughly studied recently, emission factors were estimated based mercury content in coal consumed or concentrates, different boiler types or technical types and removal efficiencies of different combinations of atmosphere pollution control devices (APCDs). For these sectors, EF in formula (1) was estimated by Formula (2). For other sectors, we directly used from literature-reported results. Typical emission factors and Hg speciation for all anthropogenic sources were listed in Table 1. PP, MSWI and IP were calculated as point sources and NI was estimated as area sources. Point sources were directly allocated into grid cells based on their latitudes and longitudes. Area sources (NI), including on-road mobile sources, residential boilers and biomass incineration, were distributed using different spatial proxies at 1×1km resolution such as road network and traffic flows information, population density, rural residential area, arable area land and woodland data.

$$E = \mathrm{AD} \times \mathrm{EF} \tag{1}$$

Where E is mercury emission, AD is the activity level, EF is the emission factors.

$$EF_i = c_i \times M_i \times R_i \times (1 - P_i) \tag{2}$$

Where EF is the emission factors, c is mercury content in fuel, M is consumption of fuel, R is mercury release rate in burning fuel, P is mercury removal rate from APCDs, i is the type of source.

2.2 Model descriptions

CMAQ-Hg version 5.0.1 was used for simulation, which was based on standard CMAQ model modified by Bullock and Brehme (2002) to include chemistry, transport and deposition of GEM, GOM and PBM. In the model, the Carbon Bond mechanism (CB05) was used as the gas-phase chemical mechanism including mercury gaseous reactions with O_3, OH, H_2O_2 and Cl_2 to generate the concentrations of photochemical oxidants. EBI (Euler

Backward Iterative) was used as a gas-phase chemistry solver in the simulations. Weather Research and Forecasting (WRF v3.9.1) model provided the meteorological fields used in CMAQ-Hg. The 6-hour global meteorological satellite data provided by the National Center for Environmental Prediction (NCEP) was used as driving data and assimilated with sounding and ground station observation data of the corresponding period. The Meteorology-Chemistry Interface Processor (MCIP v4.3) processed the WRF outputs to the CMAQ-Hg model-ready format. And dry deposition velocities of GEM and GOM were calculated by CMAQ-Hg. The dry deposition velocities of PBM was calculated similar to that of fine aerosols in Aitken and accumulation modes. Transformations of Hg are simulated with four chemical reactions which includes a compound-specific speciation for oxidized forms of Hg, aqueous-phase Hg reactions, aqueous Hg chemical equilibria, and a two-way mechanism for the sorption of dissolved oxidized Hg to elemental carbon particles (Bullock and Brehme, 2002).

2.3 Model simulations and data analysis

The modelling period was from 01 January 2014 to 31 December 2014. Annual simulations were carried out six different emission scenarios. The base case (BASE) was run with all emission from anthropogenic and natural (NAT) sources with boundary conditions (BCs). The other five scenarios selectively removed the emissions one by one from NAT, PP, MSWI, IP, BCs (C1-C5). Subtracting the results of C1-C5 from the BASE case gave effects of the mercury emission associated with these mercury sources. The CMAQ-Hg model outputs were in Network Common Data Form (netCDF). The NCAR Command Language (NCL) was used for data reading and data processing. The Model Visualization and Analysis Tool (Model-VAT) version 0.37 (available at www.abacas-dss.com) was used for data visualization. MATLAB and Microsoft Excel were used for presenting the analytical results.

3 Result and Discussion

3.1 Updated anthropogenic Mercury emission inventory in PRD to 2014

The anthropogenic mercury emission inventory in the PRD region for 2014 was presented in Table 2. The estimated total anthropogenic mercury emission was 11,939.6 kg, which was 3.7 t less than Zheng's estimation in 2008 in PRD (Zheng et al., 2011). Of all three species of mercury, GEM and GOM accounted for most of the content, with 55.0 and 42.0% respectively, while PBM is the least, with only 3.0%. The contribution of different anthropogenic sources is presented in Fig. 2a. Power plants and industrial boilers are the major mercury emission sources, responsible for 29.4 and 22.7% of the total, respectively. Emission from cement production is also substantial, accounted for approximately 22.2% of the total, followed by iron and steel production, non-ferrous metals production and municipal solid wastes incineration with contributions of 11.7, 9.0 and 4.8%, respectively. While the contribution of non-industrial anthropogenic sources, such as on-road mobile, residential boilers and biomass incineration are less than 1.0%. The speciation of mercury emission in various sectors and gridded total Hg emissions from different point sources in the PRD region for 2014 are presented in Fig. 2b and Fig. 3, further analysis of the typical anthropogenic sources is presented below.

3.1.1 Power plants—Power plants are one of the most important energy-producing industries. Although nuclear or hydroelectric power plants are gradually growing in PRD recently, most of power plants are coal-fired. In 2014, power plants' coal consumption in Guangdong province reached 106.6 million tons, and around 80.0% of them was burned in PRD (Guangdong Statistical Yearbook: http://www.gdstats.gov.cn). The total Hg emission in power plants is 3510.2 kg, of which nearly 71.0% is GEM as shown in Fig. 2b, accounted for 38.1% of all anthropogenic GEM emissions. Compared to previous study, the mercury emission of power plants in PRD for 2008 estimated by Zheng et al. (2011) was 2703 kg with a coal consumption of 62 million tons, with a 1.8 t increase (29.8%) in six years because of 37.6% increase in coal consumption. As shown in Fig. 3a, power plants are concentrated in the central PRD region and the coastal areas. Among them, the power plants that emit more than 200 kg per year are concentrated in the two most developed cities, Guangzhou and Shenzhen. However, the rising of emission from power plants was mitigated by stricter control measures. From 2005 to 2010, China's coal consumption in power plants increased by 59.0%, while the mercury emissions only rose by 10.0%, about 14t (Wang et al., 2010). Similar phenomenon also exists in PRD because of the coal-fired power plant ultra-clean emission control measures implemented by a few cities in recent years.

3.1.2 Industrial point sources—The total Hg emission from industrial point sources is 7825.4 kg, which includes four sectors: (1) Industrial boilers, 2710.7 kg; (2) Cement production, 2649.9 kg; (3) Iron and steel production, 1396.3 kg; (4) Non-ferrous metals production, 1068.5 kg (Table 2). Industrial boilers are the second largest anthropogenic emitter after power plants because of the large amount of coals consumed. Compared to previous study, the mercury emissions of industrial boilers in Guangdong province for 2014 estimated by Wu et al. (2016) was 4.7 t. Mercury emissions from industrial boilers in PRD account for approximately 60.0% of Guangdong province. Zheng et al. (2011) estimated mercury emissions from coal combustion (excluding coal-fired power plants) in PRD for 2008, which were nearly 2000 kg, more than 700 kg (35.2%) mercury emission increased during six years. Cement production has the highest GOM and PBM emission of all, accounting for 24.9 and 30.7%. Wu et al. (2016) estimated mercury emissions from cement production in Guangdong province for 2014 (6.9 t), which was the largest emitter in Guangdong. However, in the highly urbanized PRD, cement production are not so dominant, only 38.4% mercury emission of total cement production of Guangdong province. And for iron and steel production and non-ferrous metals production, GOM is the major species, accounting for 65.0 and 49.0% (Fig. 2b). As shown in Fig. 3b, industrial boilers are widely distributed in PRD region, all cities have Hg emissions from these sectors. In addition, it is obviously that high Hg emissions regions from IP are concentrated in cities such as Foshan, Dongguan, Zhongshan, Jiangmen and Qingyuan. In the past decade, with the improvement of industrial technology and energy substitution, mercury emissions from these industries have been gradually reduce (Wu et al., 2006; Zhang et al., 2015). In China, the mercury emission reduction in industrial boilers, cement production and metal smelting industry were 27.9, 23.7 and 47.0% between 2003 and 2010. In the long run, mercury emissions from these industries will be more effectively controlled.

3.1.3 Municipal solid wastes incineration—Over the past decade, the amount of municipal solid wastes (MSW) has risen sharply at an annual rate of 10.0%. In 2010, the total amount of incineration disposal in PRD was 3.6 million tons, accounting for 31.0% of the total amount of MSW (Chen et al., 2013). Due to the lack of mercury control on municipal solid wastes incineration (MSWI), the mercury emission from MSWI has a sharp increase. In 2014, total Hg emission from MSWI in PRD is 578.3 kg, of which almost 80.0% is GOM, accounted for 8.8% of all anthropogenic GOM emissions. The result is slightly lower than the study (Total Hg emission 770 ± 65.5 kg, GOM 688 ± 65.5 kg) reported by Chen et al. (2013). The reason for this difference is that APCDs used in MSWI currently influence transformation of mercury speciation and improve mercury removal efficiency. Fig. 3c shows the distribution of MSWI in PRD region. In Guangzhou, Dongguan, Foshan, Zhuhai and Shenzhen, concentrated all the MSWI of Guangdong province. Similar to the distribution of PP, MSWI with the largest Hg emissions are also concentrated in the two most populated cites, Guangzhou and Shenzhen. Due to relatively abundant land resources, low population density and incomplete waste incineration technologies in other cities, MSWI are rarely built and operated.

3.1.4 Non-industrial anthropogenic sources—Non-industrial anthropogenic sources includes on-road mobile, residential boilers and biomass incineration. Total Hg emissions from on-road mobile are estimated to be 16.2 kg, while residential boilers and biomass incineration only 5.1 and 4.4 kg. All of them are mostly released as GEM, accounting for 50.0% in on-road mobile and 72.0% in residential boilers and biomass incineration. However, the non-industrial Hg emission accounts for less than 1.0% of the total anthropogenic Hg emission, much smaller than emissions from industry sources.

3.2 Model Validation

3.2.1 WRF results—The performance of the WRF model was evaluated by comparing hourly mean predicted and measured values at the Sugang and Yuanling monitoring sites Table 3. The average Pearson correlation coefficient (R) and Index of Agreement (IOA) for relative humidity and temperature were about 0.8 or greater. For wind speed, R and IOA were greater than 0.5, but modeled wind speeds were much higher (normalized mean bias, NMB: 132%) at Sugang. This may be due to the fact that the WRF model's ground surface patch file was not updated in time. In the PRD region, the observations of annual rainfall was 2234mm (Guangzhou meteorological data: www.data.tqyb.com), while were close to our predicted rainfall in the same area (2160mm). Overall, the WRF simulation results are still within an acceptable error range.

3.2.2 Atmospheric mercury concentration—The spatial distribution of annual mean surface concentrations and total depositions of GEM, GOM and PBM simulated in the base year 2014 are shown in Fig. 4. The simulated annual average concentration of total atmospheric mercury is 3.8 ng m^{-3}. GEM, GOM and PBM were in the ranges of 3.1–5.6, 0.1–2.4 and 0.1–1.3 ng m^{-3}. On average, GEM constituted 92.0% of the total atmospheric mercury with the contribution going down to a minimum of 55.9% near high emission areas, which was mainly in the central and western areas of PRD (Fig. 4a). In comparison, GOM and PBM have low concentrations, only 4.5 and 3.4% of the total, respectively. These result

are quite consistent with earlier model predictions (Lin et al., 2010; Li et al., 2011; Wang et al., 2014; Zhu et al., 2015). The fraction of GOM and PBM is typically greater at locations near point sources because of the emission speciation (nearly 46.0% of mercury is emitted as GOM and PBM), and both decreases rapidly away from source locations due to their relatively shorter atmospheric lifetimes (Fig. 4b, c). The model results in BASE scenario were compared to observations to give a preliminary evaluation of model performance. Due to the very limited long-term mercury monitoring in PRD and more than 90.0% of the total atmospheric mercury is TGM/GEM, the public reported TGM/GEM concentration measurements were used to assess the model performance (the data of PBM concentration was not found in the public released document in PRD). Table 4 lists the comparisons of model results with observations. The simulated GEM is consistent with observations with a relative bias of −24.2–16.3%. In Guangzhou remote areas, the observations of Guangzhou rural site and Wangqingsha were 10.3–16.3% lower than our simulations. The overestimation of our result is because two observation sites are located at a coastal area in Nansha district with only one or two month of winter measurement data, which are highly affected by the atmospheric mercury transmission from northern provinces during the winter when the north wind prevails. The emissions from northern provinces such as Hunan, Jiangxi in cement production (−81.6%, +98.5%) and non-ferrous metal smelting (Zn smelting (−63%, +81%), Pb smelting (−61%, +89%)) had a high uncertainties (Tian et al., 2015, Wu et al., 2016). Therefore, the overestimated emssions from outside PRD (mainly from nothern provinces) caused the high model results to the background sites. In Guangzhou urban site and Mt. Dinghu, the model underestimated by about 18.5%−24.2%. These two sites are located where the regional large point sources around which highly affected the observations.

3.2.3 Mercury deposition—The simulated total mercury deposition was 163.6 μg·m^{-2}·yr^{-1}, with 46.4 μg·m^{-2}·yr^{-1} of total dry deposition and 117.3 μg·m^{-2}·yr^{-1} of total wet deposition. The net dry deposition of GEM was only 0.21 μg·m^{-2}·yr^{-1} (Fig. 4d), accounted for 0.4% of the total dry deposition, which was lower than previous studies (Wang et al., 2014; Zhu et al., 2015) because the bidirectional surface exchange of mercury was used by the model CMAQ-Hg v5.0.1. The results of GEM in dry deposition are the flux of mercury between the atmosphere and the natural surface. In rural and remote areas, atmospheric mercury from dry deposition and natural surface emission are close to equilibrium, and the flux of mercury in most of areas tends to zero (Bash et al., 2007). The dry deposition of GOM range from 9.3–638.9 μg·m^{-2}·yr^{-1}, with an average of 37.3μg·m^{-2}·yr^{-1} (80.7%), which was the dominant fraction of mercury dry deposition. PBM contributed 8.9 μg·m^{-2}·yr^{-1} (19.1%) to total dry deposition with a range of 2.5–411.2 μg·m^{-2}·yr^{-1}. The distribution of the dry deposition of GOM and PBM resembled the spatial pattern of urban areas in PRD as result of high concentration of GOM and PBM there (Fig. 4e, f). The wet deposition was dominated by GOM (67.4%) and PBM (32.5%) (Fig. 4h, i). The distribution of wet deposition is obviously influenced by both precipitation and emissions. The wet deposition of GEM was negligible due to its low solubility in water (Fig. 4g). The observation data for mercury deposition is limited in PRD and all available observations in PRD region were used to verify the model performance (Table 5). In Guangzhou urban areas, the wet deposition and dry deposition were 148.2 μg·m^{-2}·yr^{-1} (86.7–164.6 μg·m^{-2}·yr^{-1}) and 55.2

μg·m^{-2}·*yr*$^{-1}$ (21.7–70.6 μg·m^{-2}·*yr*$^{-1}$) while the wet deposition and dry deposition measured by Huang et al. (2016) were 145.8 μg·m^{-2}·*yr*$^{-1}$ and 58.6 μg·m^{-2}·*yr*$^{-1}$ respectively. The modelled and predicted results were quite close. In the Dinghushan site, which is a rural area of PRD, the estimated annual wet deposition was 113.6 μg·m^{-2}·*yr*$^{-1}$ (75.3–134.2 μg·m^{-2}·*yr*$^{-1}$), which was 9.2 μg·m^{-2}·*yr*$^{-1}$ higher than the observations in 2012 by Huang (Huang et al., 2016), while simulated dry deposition (45.6 μg·m^{-2}·*yr*$^{-1}$) was lower than the observation (54.6 μg·m^{-2}·*yr*$^{-1}$). The modelled mercury wet deposition in the PRD region is in the same magnitude as the observations, and the 2.0–11.0% overestimation is mainly due to the fact that the rainfall in 2014 is about 20.0% higher than the average annual precipitation in 2010–2013 (Table 5). Fig. 5 is a linear regression of annual wet deposition and rainfall in the PRD region. The coefficient of determination R of the fitted curve was about 0.85, which showed the consistent distribution of annual wet deposition and rainfall. In 2014, there was a heavy rain disaster in southern China, the northern and western Guangdong province suffered more than the central PRD region, rainfall in the entire PRD region was higher than average. Overall, the model simulation did well in reflecting the concentration and deposition of the atmospheric mercury in the PRD and is suitable for further source apportionment analysis.

3.3 Source apportionment

3.3.1 Boundary conditions (BCs)—Fig. 6 summarize annual and seasonal contributions of different sources to atmospheric mercury concentration and deposition in the PRD. The impacts of boundary conditions (BCs) were significant for atmospheric mercury pollution in the PRD, which indicates the contribution of mercury emissions from beyond the study domain including the global background. BCs contributed 31.5% of the annual averaged total Hg concentration, while the contribution of the GEM is most. This is because GEM has long lifetime in the atmosphere and can be transported far beyond the source regions. BCs contributed 29.3% to annual wet deposition of mercury in the PRD. However, the contribution to dry deposition of BCs was 32.3%, a little higher than wet deposition. BCs' contribution has significant seasonal variations. For dry deposition, due to the monsoon and large amount of coal burning in Northern Provinces, the impacts of BCs in spring and winter were larger than in summer and autumn. However, contributions of BCs to wet deposition were relatively even in different seasons. The contributions of BCs in summer and autumn were slightly higher than that in spring and winter due to the difference in rainfall.

Fig. 7b showed the spatial distribution of mercury deposition contributed by BCs, we can see effects on THg deposition in the Northern Guangdong areas (Qingyuan, Shaoguan, Heyuan and northern Guangzhou areas according to Fig. 1) were much larger than other areas. Different dominant monsoons in seasons will cause different effects on the domain with different boundaries. In the winter, the emissions from the northern Hunan and Jiangxi provinces had a significant impact on the PRD when the north wind dominated. In the summer, when the south wind dominated, the background concentration of global mercury pool will transmitted from the offshore region to the PRD. For the whole year, BCs contributed 20.0–45.0% in northern areas, while only 5.0–15.0% was contributed to southern coastal areas. Zhu et al. (2015) estimated the contribution of BCs to mercury concentrations (18.7%) in Eastern China and depositions (dry deposition 15.4%, wet

deposition 32.3%), and the results were lower than this study. One of the reasons is the much higher BCs from China mainland than the global mercury pool. Moreover, the PRD region is relatively much smaller than the eastern china area and tends to be affected more by the boundary transports.

3.3.2 Natural sources (NAT)—The contribution of NAT to total mercury concentration, dry deposition and wet deposition was 15.0, 15.0 and 24.0%, respectively. Emission from NAT has significant seasonal variations, between 27.0% in summer time and 7.2% in winter time. In summer lower average atmospheric GEM concentration, higher temperature, better diffusion conditions and larger turbulence all enhanced the mercury evasion from land surface. As shown in Fig. 7c, natural emissions in the PRD is much evenly distributed compared to anthropogenic sources, there is no significant concentration of high-emitting regions. In addition, NAT contributed 19.5% of the total deposition, while anthropogenic sources contributed 49.7%. So in the PRD, anthropogenic emissions are dominant.

3.3.3 Power plants (PP)—Power plants, having close to 25.0% of the total emission, contributed 18.9% to atmospheric mercury concentration. PP were also responsible for 22.0 and 14.4% of dry and wet deposition, which resulted from its significant impacts on GOM concentrations. Fig. 7d shows the relative difference between PP scenario and BASE scenario. Shutting down the emission from power plants obviously decreased the THg deposition in central and southern PRD (Foshan, Guangzhou, Zhuhai, Zhongshan and northern Dongguan). According to the Guangdong Statistical yearbook, nearly 70.0% of Guangdong's power plants are concentrated in these areas. The large number and respective capacity of power plants resulted in a high THg deposition in these regions. With the increase of energy consumption, the number of coal-fired power plants with capacities larger than 1000MW is still growing in the PRD. Higher emission intensity from PP led to a higher influence on atmospheric mercury pollution if no further control measures are taken.

3.3.4 Municipal solid waste incineration (MSWI)—The contribution of MSWI to total mercury concentration, dry deposition and wet deposition was 11.3, 10.9 and 9.7%, respectively. The high contribution mostly appeared in summer and autumn. MSWI were the third largest sectors among all anthropogenic sources and they were treated as point sources in the model. As Hg emission from MSWI was mainly in the form of GOM with a percentage of 78.0%, MSWI has a higher contribution to GOM than to GEM and PBM. Fig. 7e shows the relative difference between MSWI scenario and BASE scenario. In PRD, MSWI had little impact in most of areas except Foshan, Guangzhou and parts of Dongguan, Shenzhen, Huizhou and Zhuhai, because these urbanized areas are densely populated, with high waste production and large waste disposal facilities. Although the contribution of MSWI was lower than sectors such as PP and IP, the potential of MSWI is attracting increased attention due to the fast growth of municipal waste production and incineration treatment in the PRD.

3.3.5 Industrial point sources (IP)—IP was the largest anthropogenic emission source in PRD amounted for 65.5% of the total atmospheric mercury emission. Moreover, 46.7% of the total mercury emitted from IP was GOM, which made up 72.2% of the total GOM

emissions in PRD. Also, IP was the largest source of PBM with 73.7% of the total PBM emission in PRD. Due to the large quantity of GOM and PBM which can be deposited fast near the emission sources through dry and wet deposition, IP contributed 19.8 and 22.7% of annual dry and wet deposition. The contributions of IP to mercury deposition in winter were higher than other seasons. As the seasonal variations of important anthropogenic sources are small, significant reductions of mercury emission from NAT in winter is the dominant reason. As shown in Fig. 7f, shutting down the emission from IP had great impacts in the domain, especially in the central and north-eastern PRD. In the central PRD, such as Foshan, Guangzhou and Zhaoqing, a large amount of cement productions and industrial boilers lead to high mercury emissions. Cement productions are also important mercury emitters. They emitted approximately 2.7 t mercury in PRD, accounting for 22.2% of the total Hg emission, nearly 50.0% of which came from the above three cities. Non-ferrous metals production and Iron and steel production emitter about 2.5 t mercury, accounting for 20.6% of the total Hg emission. They are mainly in the northern cities of PRD such as Heyuan, Qingyuan and Shaoguan. So in these areas, shutting down the emission from IP obviously decreased the THg deposition.

3.4 Implications for mercury emission control

In the densely populated PRD region, bioaccumulation is one of the most important issues to be considered to the harmful effects of mercury on human body. Therefore, total mercury deposition is the most important factor for mercury control. Areas with total mercury deposition over 250 $\mu g \cdot m^{-2} \cdot yr^{-1}$ include Foshan, Guangzhou, parts of Dongguan and Huizhou in the central PRD, parts of Zhaoqing and Foshan in the western PRD and parts of Qingyuan and Heyuan in the northern PRD. These regions should be the priority of mercury pollution control (Fig. 7a). In the central PRD, power plants should be first controlled. At present, Chinese government has put forward the ultra-low emission (ULE) for thermal power units, which requires the emission limit values of dust, NO_x and SO_2 are 5.0 mg m^{-3}, 35.0 mg m^{-3} and 50.0 mg m^{-3}, in some provinces including Guangdong. The installation of selective catalytic reduction (SCR), electrostatic precipitator (ESP), wet flue gas desulfurization (WFGD) and wet electrostatic precipitator (WESP) was completed before 2018 and mercury emissions will be reduced by about 40.0–50.0% (due to the increasing energy consumption in power plants, the reduction will not too high) in the near future which will reduce mercury deposition by about 2 t. Power plants in Guangzhou, Foshan and Shenzhen emitted more than 200 kg of mercury per year. Ultra-low measures implemented at these power plants will control mercury emissions more effectively. For further reduction, other sectors should be considered and cement production should be the second priority. The deposition will be reduced about 0.5 t if controlling 30.0% of emissions in this sector. In the northern and western PRD, non-ferrous metals production and iron and steel production are important emitters. Controlling 30.0% of emissions from metals production will reduce 0.4 t mercury deposition in the PRD, especially at the steel smelters in Heyuan and Zhaoqing and the lead and zinc smelters in Foshan. Finally, the waste incineration plants also need to control. In the northern part of Guangzhou and Shenzhen, the implementation of strict mercury emission control measures for the two largest MSWI in the PRD will reduce mercury deposition by 0.6 t with 30.0% of emission reducing. However, as municipal solid

waste continues to increase, it is urgent to improve the waste incineration flue gas emission control technology.

4 Conclusion

In this study, the total anthropogenic mercury emissions in PRD for 2014 are estimated around 11,939.6 kg, of which 55.0% released as GEM, 42.0% as GOM and 3.0% as PBM. Power plants and industrial boilers are the two largest emission sources, accounting for 29.4 and 22.7% of the total anthropogenic emissions. It is noteworthy that mercury emission from municipal solid waste incineration is 578.3kg, nearly 5.0% of the total. The rapid growth of MSWI and its uneven distribution in China pose a huge challenge to the management of solid wastes associated with urbanization. Other industrial sources such as cement production, iron and steel production and non-ferrous metal production account for 22.2, 11.7 and 9.0% respectively. Non-industrial anthropogenic sources, including on-road mobile residential boilers and biomass incineration, are less than 1.0% of the total. Therefore, industrial atmospheric mercury emission control is the most important, especially in some high-emission mercury industries such as PP, IP and MSWI.

The simulation of atmospheric mercury in PRD was conducted using CMAQ-Hg with the updated 2014 mercury emission inventory. The base simulation results were consistent with the measurements of atmospheric mercury at most of the sites in PRD, and the deposition levels are also compatible with observations at other sites in China. Because of the high anthropogenic mercury emission in Southern China provinces and the small area of PRD, BCs with a high contribution of 31.7% for annual average Hg concentration. However, NAT was only responsible for 15.2% in the region, which contributed more in summer and autumn than that in spring and winter. Among the anthropogenic sources, IP and PP were the largest contributors to mercury concentration with contributions of 23.0 and 18.8%. The contributions showed seasonal variation. The largest contributor, IP have higher contributions in autumn and winter than that in spring and summer. The estimated total deposition in the model domain is 163.6 μg m^{-2} yr^{-1}, 28.4% for dry deposition and 71.6% for wet deposition. For dry deposition, three anthropogenic sources IP (19.8%), PP (22%) and MSWI (10.9%) together contributed nearly 53.0% of the total, while the contribution from NAT was only 15.0%. For wet deposition, due to the rainfall in PRD, the impact of BCs (29.3%) is weaker than its dry deposition. The contribution of anthropogenic sources is less than 50.0%, while the contribution of NAT is 24.0%, higher than its dry deposition.

Due to the considerable contribution to mercury deposition in the outside PRD area, a coordinated regional emission reduction effort is important for effectively reducing mercury deposition in the PRD. In addition, power plants are the two largest contributor in cities such as Foshan, Guangzhou and Shenzhen in the central PRD. The ultra-low emission (ULE) for thermal power units need to be strengthened. For industrial point sources, cement production, non-ferrous metal production and iron and steel production have great impacts on the northern and western PRD region, such as Qingyuan, Heyuan and Zhaoqing. It is necessary to strengthen control measures for fume emission in these industries. In some large populated and developed areas of PRD, municipal solid waste incineration is also an important source of mercury pollution. Increasing municipal solid wastes will cause great

trouble to the industry in controlling mercury emission, the control of mercury emissions from MSWI is also urgent and essential.

Acknowledgement

This work was supported by the Natural Science and Technology Foundation of Guangdong Province, China (2016A020221001), National research program for key issues in air pollution control (No.DQGG0301), The National Key Research and Development Program of China (No.2016YFC0207605) and the Fundamental Research Funds for the Central Universities (No.D2160320 and D2170150).

References

Bash JO, Bresnahan P, Miller DR (2007). Dynamic surface interface exchanges of mercury: A review and compartmentalized modeling framework. Journal of Applied Meteorology and Climatology, 46(10): 1606–1618

Bullock OR, Atkinson D, Braverman T, Civerolo K, Dastoor A, Davignon D, Ku JY, Lohman K, Myers TC, Park RJ, Seigneur C, Selin NE, Sistla G, Vijayaraghavan K (2008). The North American Mercury Model Intercomparison Study (NAMMIS): Study description and model-to-model comparisons. Journal of Geophysical Research-Atmospheres, 113(D17): 17

Bullock OR, Atkinson D, Braverman T, Civerolo K, Dastoor A, Davignon D, Ku JY, Lohman K, Myers TC, Park RJ, Seigneur C, Selin NE, Sistla G, Vijayaraghavan K (2009). An analysis of simulated wet deposition of mercury from the North American Mercury Model Intercomparison Study. Journal of Geophysical Research-Atmospheres, 114: 12

Bullock OR, Brehme KA (2002). Atmospheric mercury simulation using the CMAQ model: formulation description and analysis of wet deposition results. Atmospheric Environment, 36(13): 2135–2146

Chen LG, Liu M, Fan RF, Ma SX, Xu ZC, Ren MZ, He QS. (2013). Mercury speciation and emission from municipal solid waste incinerators in the Pearl River Delta, South China. Science Of the Total Environment, 447: 396–402

Chen LG, Liu M, Xu ZC, Fan RF, Tao J, Chen DH, Zhang DQ, Xie DH, Sun JR (2013). Variation trends and influencing factors of total gaseous mercury in the Pearl River Delta-A highly industrialised region in South China influenced by seasonal monsoons. Atmospheric Environment, 77: 757–766

Holloway T, Voigt C, Morton J, Spak SN, Rutter AP, Schauer JJ (2012). An assessment of atmospheric mercury in the Community Multiscale Air Quality (CMAQ) model at an urban site and a rural site in the Great Lakes Region of North America. Atmospheric Chemistry And Physics, 12(15): 7117–7133

Holmes CD, Jacob DJ, Mason RP, Jaffe DA (2009). Sources and deposition of reactive gaseous mercury in the marine atmosphere. Atmospheric Environment, 43(14): 2278–2285

Hu YA, Cheng HF (2016). Control of mercury emissions from stationary coal combustion sources in China: Current status and recommendations. Environmental Pollution, 218: 1209–1221 [PubMed: 27596303]

Huang MJ, Deng SX, Dong HY, Dai W, Pang JM, Wang XM (2016). Impacts of Atmospheric Mercury Deposition on Human Multimedia Exposure: Projection from Observations in the Pearl River Delta Region, South China. Environmental Science and Technology, 50(19): 10625–10634 [PubMed: 27577539]

Keeler GJ, Landis MS, Norris GA, Christianson EM, Dvonch JT (2006). Sources of mercury wet deposition in eastern Ohio, USA. Environmental Science and Technology, 40(19): 5874–5881 [PubMed: 17051773]

Li Z, Xia C H, Wang X M, Xiang Y R, Xie Z Q (2011). Total gaseous mercury in Pearl River Delta region, China during 2008 winter period. Atmospheric Environment, 45(4): 834–838

Liang S, Xu M, Liu Z, Suh S, Zhang T Z (2013). Socioeconomic Drivers of Mercury Emissions in China from 1992 to 2007. Environmental Science and Technology, 47(7): 3234–3240 [PubMed: 23473539]

Lin CJ, Pan L, Streets DG, Shetty SK, Jang C, Feng X, Chu HW, Ho TC (2010). Estimating mercury emission outflow from East Asia using CMAQ-Hg. Atmospheric Chemistry And Physics, 10(4): 1853–1864

Lin CJ, Shetty SK, Pan L, Pongprueksa P, Jang C, Chu HW (2012). Source attribution for mercury deposition in the contiguous United States: Regional difference and seasonal variation. Journal Of the Air and Waste Management Association, 62(1): 52–63 [PubMed: 22393810]

Lohman K, Seigneur C, Edgerton E, Jansen J (2006). Modeling mercury in power plant plumes. Environmental Science and Technology, 40(12): 3848–3854 [PubMed: 16830552]

Sakata M, Marumoto K (2005). Wet and dry deposition fluxes of mercury in Japan. Atmospheric Environment, 39(17): 3139–3146

Selin NE, Jacob DJ (2008). Seasonal and spatial patterns of mercury wet deposition in the United States: Constraints on the contribution from North American anthropogenic sources. Atmospheric Environment, 42(21): 5193–5204

Streets DG, Hao JM, Wu Y, Jiang JK, Chan M, Tian HZ, Feng XB (2005). Anthropogenic mercury emissions in China. Atmospheric Environment, 39(40): 7789–7806

Sutton MA, Burkhardt JK, Guerin D, Nemitz E, Fowler D (1998). Development of resistance models to describe measurements of bi-directional ammonia surface-atmosphere exchange. Atmospheric Environment, 32(3): 473–480

Tian HZ (2015). Quantitative assessment of atmospheric emissions of toxic heavy metals from anthropogenic sources in China: historical trend, spatial distribution, uncertainties, and control policies. Atomspheric Chemistry and Physics, 15: 10127–10147

Wang L, Wang SX, Zhang L, Wang YX, Zhang YX, Nielsen C, McElroy MB, Hao JM (2014). Source apportionment of atmospheric mercury pollution in China using the GEOS-Chem model. Environmental Pollution, 190: 166–175 [PubMed: 24768744]

Wang LT, Wei Z, Wei W, Fu JS, Meng CC, Ma SM (2015). Source apportionment of PM2.5 in top polluted cities in Hebei, China using the CMAQ model. Atmospheric Environment, 122: 723–736

Wang S B, Luo K L (2017). Atmospheric emission of mercury due to combustion of steam coal and domestic coal in China. Atmospheric Environment, 162: 45–54

Wang SX, Zhang L, Wang L, Wu QR, Wang FY, Hao JM (2014). A review of atmospheric mercury emissions, pollution and control in China. Frontiers of Environmental Science and Engineering, 8(5): 631–649

Wang YJ, Duan YF, Yang LG, Zhao CS, Xu YQ (2010). MERCURY SPECIATION AND EMISSION FROM THE COAL-FIRED POWER PLANT FILLED WITH FLUE GAS DESULFURIZATION EQUIPMENT. Canadian Journal of Chemical Engineering, 88(5): 867–873

Wesely M L, Hicks BB (2000). A review of the current status of knowledge on dry deposition. Atmospheric Environment, 34(12–14): 2261–2282

Wu QR, Wang SX, Li GL, Liang S, Lin CJ, Wang YF, Cai SY, Liu KY, Hao JM (2016). Temporal Trend and Spatial Distribution of Speciated Atmospheric Mercury Emissions in China During 1978–2014. Environmental Science and Technology, 50(24): 13428–13435 [PubMed: 27993067]

Wu Y, Wang SX, Streets DG, Hao JM, Chan M, Jiang JK (2006). Trends in anthropogenic mercury emissions in China from 1995 to 2003. Environmental Science and Technology, 40(17): 5312–5318 [PubMed: 16999104]

Zhang L, Wang SX, Wang L, Wu Y, Duan L, Wu QR, Wang FY, Yang M, Yang H, Hao JM, Liu X (2015). Updated Emission Inventories for Speciated Atmospheric Mercury from Anthropogenic Sources in China. Environmental Science and Technology, 49(5): 3185–3194 [PubMed: 25655106]

Zhang XT, Siddiqi Z, Song XJ, Mandiwana KL, Yousaf M, Lu JL (2012). Atmospheric dry and wet deposition of mercury in Toronto. Atmospheric Environment, 50: 60–65

Zhang Y, Jaegle L, van Donkelaar A, Martin RV, Holmes CD, Amos HM, Wang Q, Talbot R, Artz R, Brooks S, Luke W, Holsen TM, Felton D, Miller EK, Perry KD, Schmeltz D, Steffen A, Tordon R, Weiss-Penzias P, Zsolway R. (2012). Nested-grid simulation of mercury over North America. Atmospheric Chemistry And Physics, 12(14): 6095–6111

Zhao Y, Zhong H, Zhang J, Nielsen CP (2015). Evaluating the effects of China's pollution controls on inter-annual trends and uncertainties of atmospheric mercury emissions. Atmospheric Chemistry And Physics, 15(8): 4317–4337

Zheng JY, Ou JM, Mo ZW, Yin SS (2011). Mercury emission inventory and its spatial characteristics in the Pearl River Delta region, China. Science Of the Total Environment, 412: 214–222

Zhu J, Wang T, Bieser J, Matthias V (2015). Source attribution and process analysis for atmospheric mercury in eastern China simulated by CMAQ-Hg. Atmospheric Chemistry And Physics, 15(15): 8767–8779

Zhu J, Wang T, Talbot R, Mao H, Yang X, Fu C, Sun J, Zhuang B, Li S, Han Y, Xie M (2014). Characteristics of atmospheric mercury deposition and size-fractionated particulate mercury in urban Nanjing, China. Atmospheric Chemistry and Physics, 14(5): 2233–2244

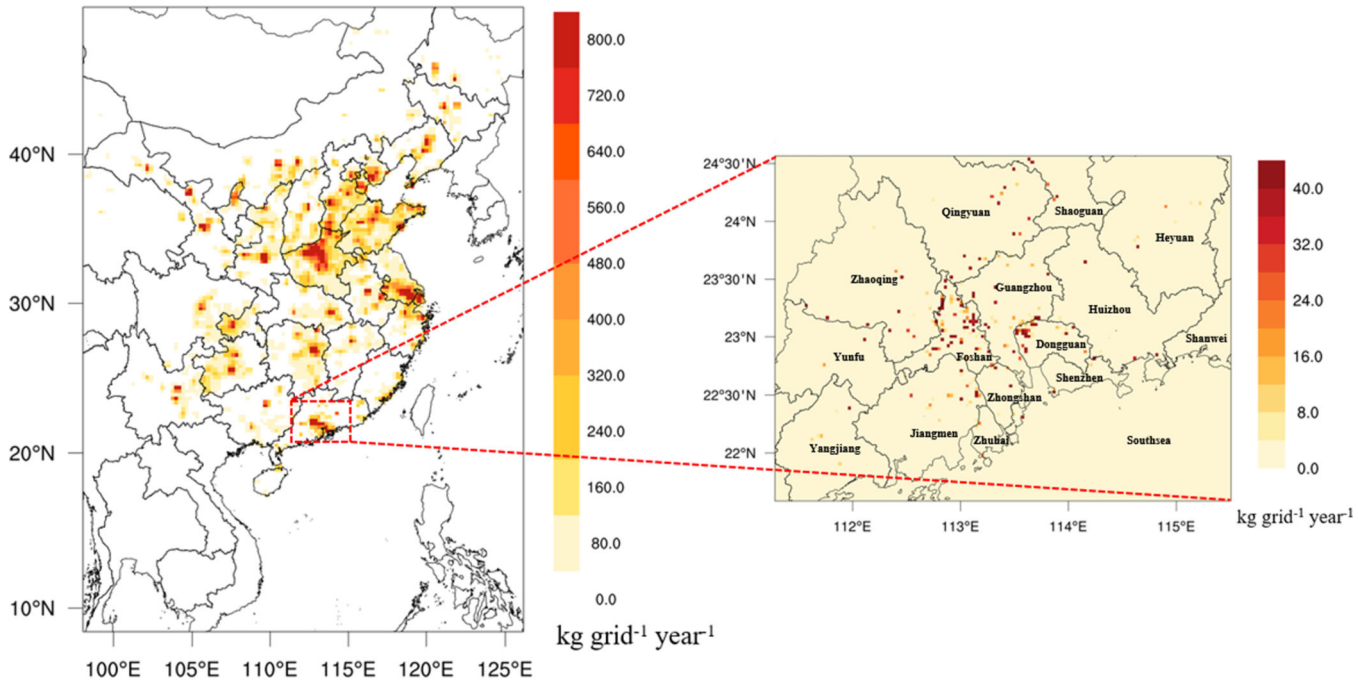

Fig. 1.
Study domains with annual total mercury emissions

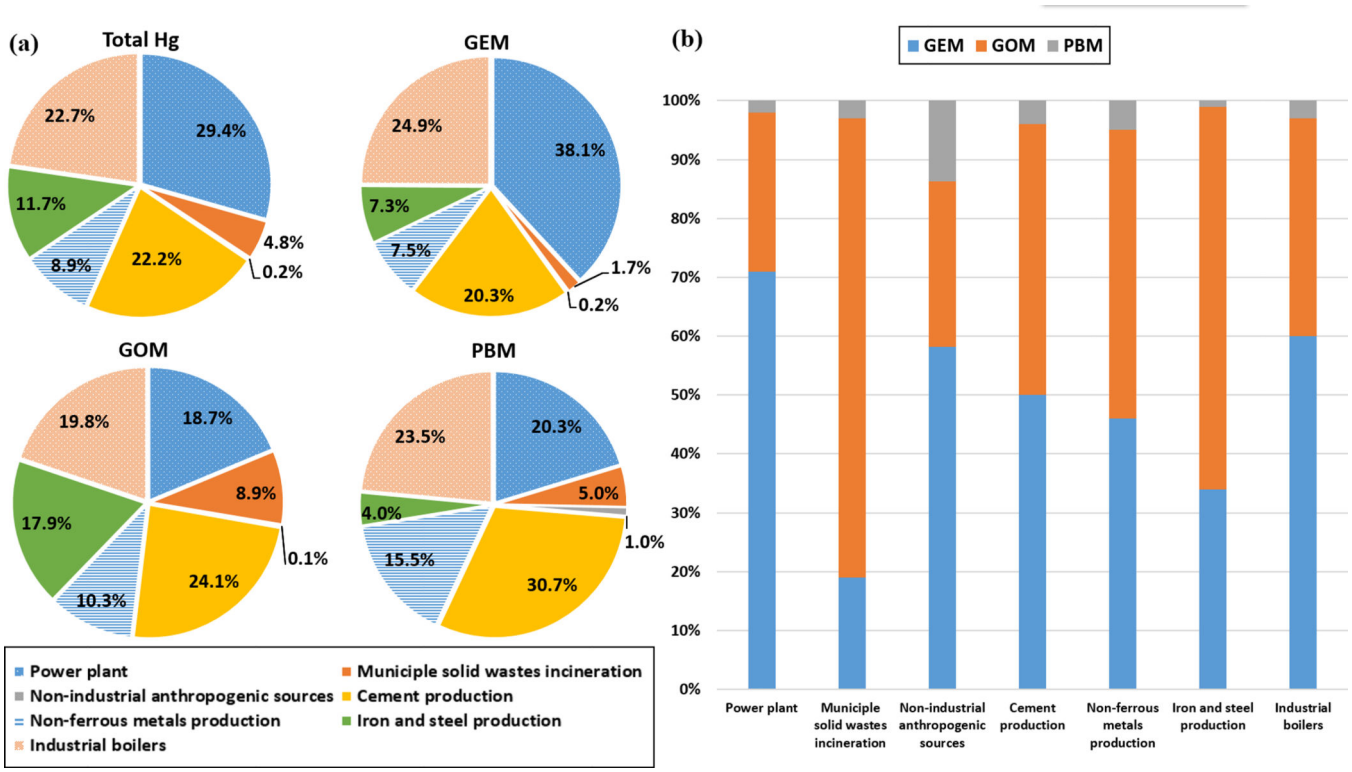

Fig. 2.

(a) Proportion of different anthropogenic Hg emissions sources, (b) Contribution of different mercury species in various sectors

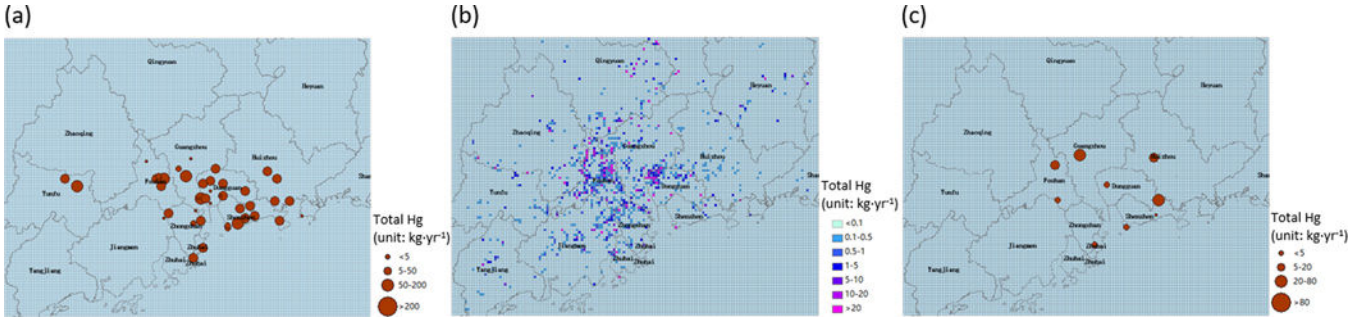

Fig. 3.

Gridded Hg emissions from (a) power plants, (b) industrial boilers, (c) municipal solid waste incineration

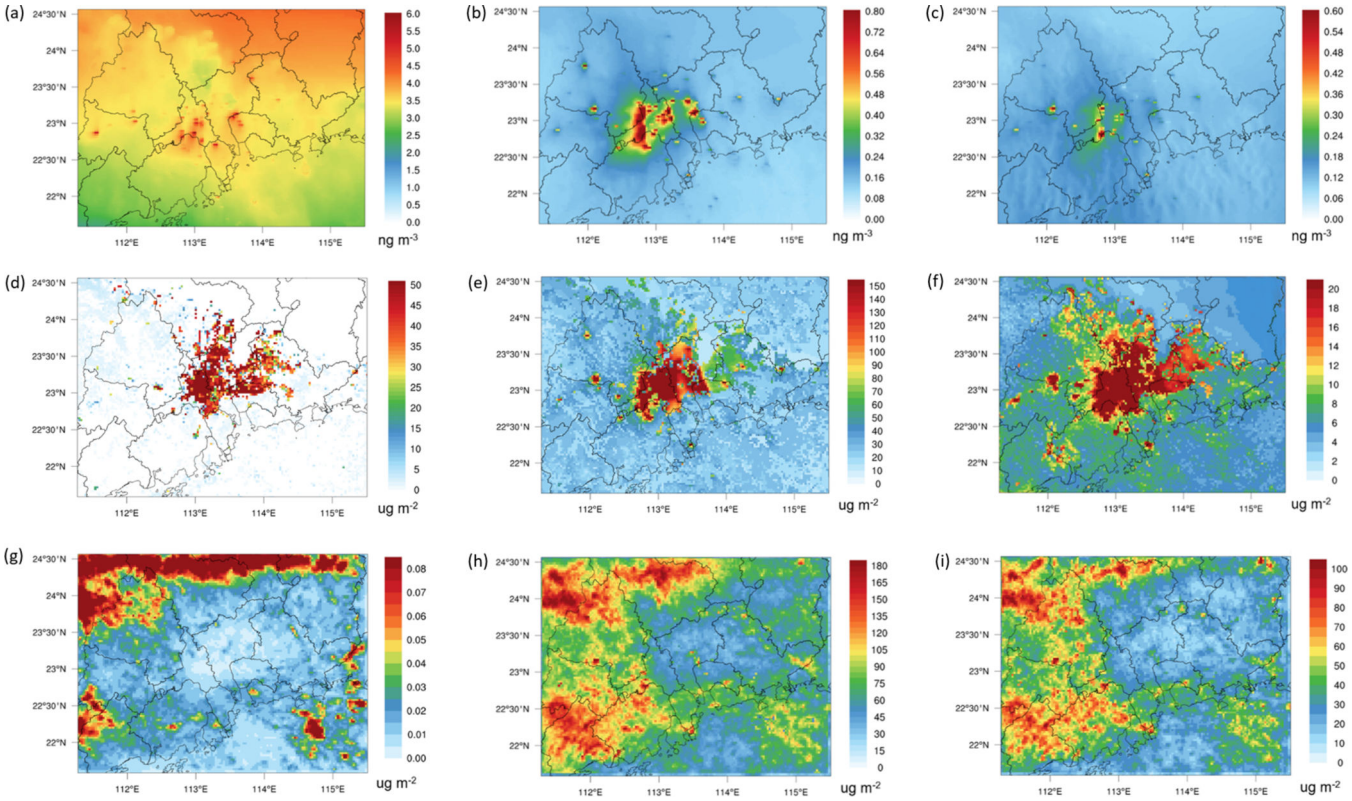

Fig. 4.

Simulated annual average concentration of (a) GEM, (b) GOM and (c) PBM; annual dry deposition of (d) GEM, (e) GOM and (f) PBM; and annual wet deposition of (g) GEM, (h) GOM and (i) PBM in PRD for 2014

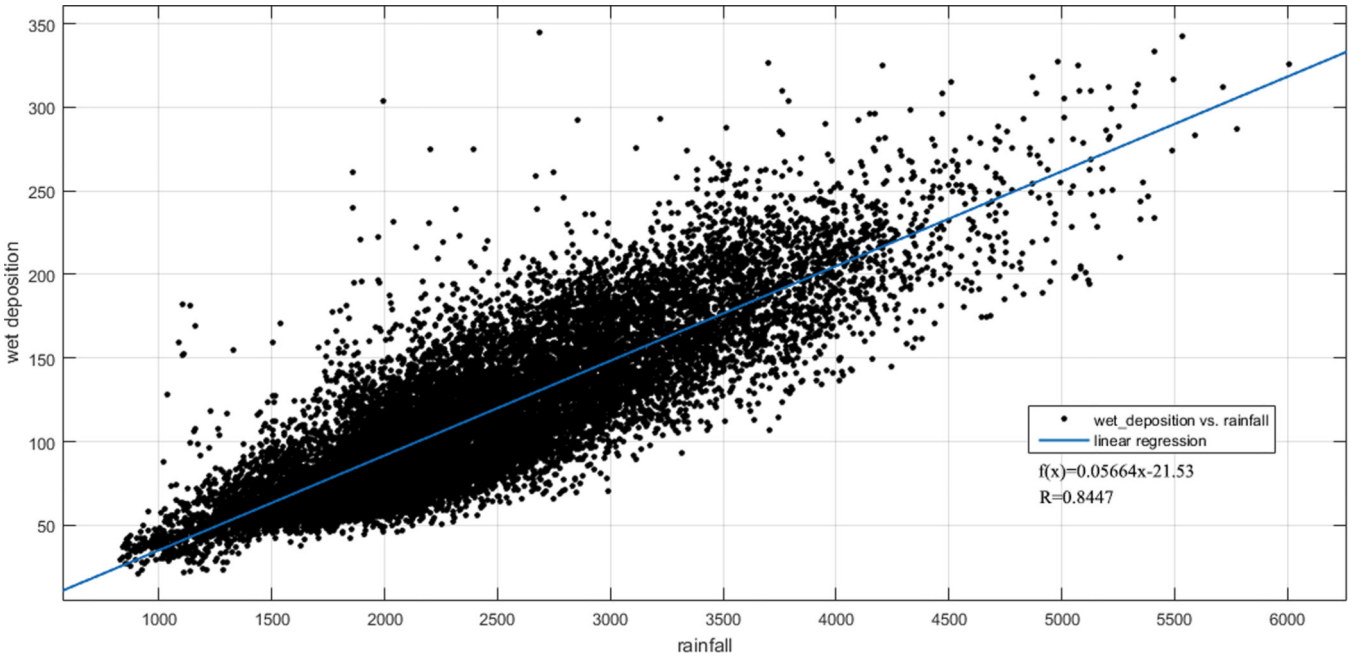

Fig. 5.
Verification of annual mercury wet deposition and rainfall

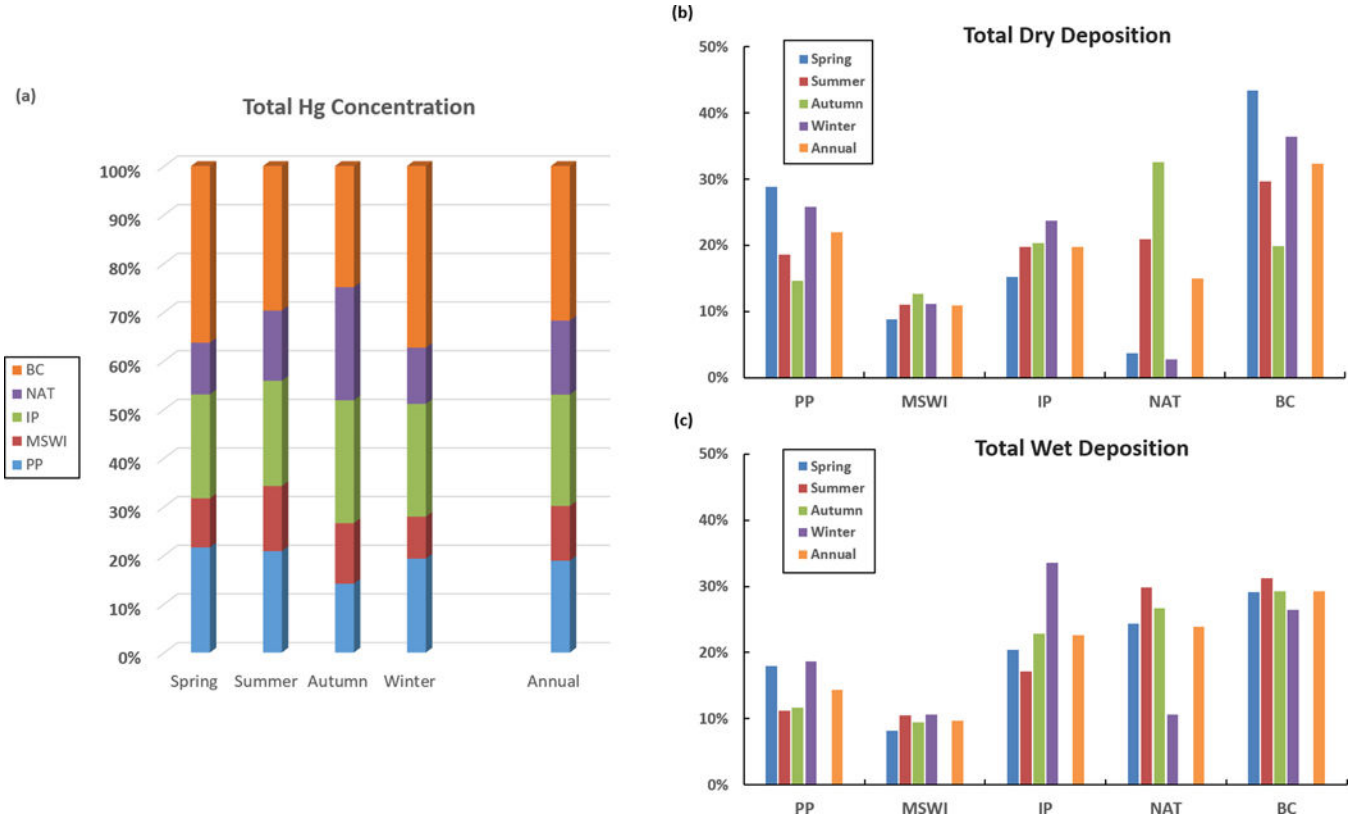

Fig. 6.

Source contributions to seasonal and annual averaged (a) total mercury concentrations, (b) total mercury dry depositions and (c) wet depositions

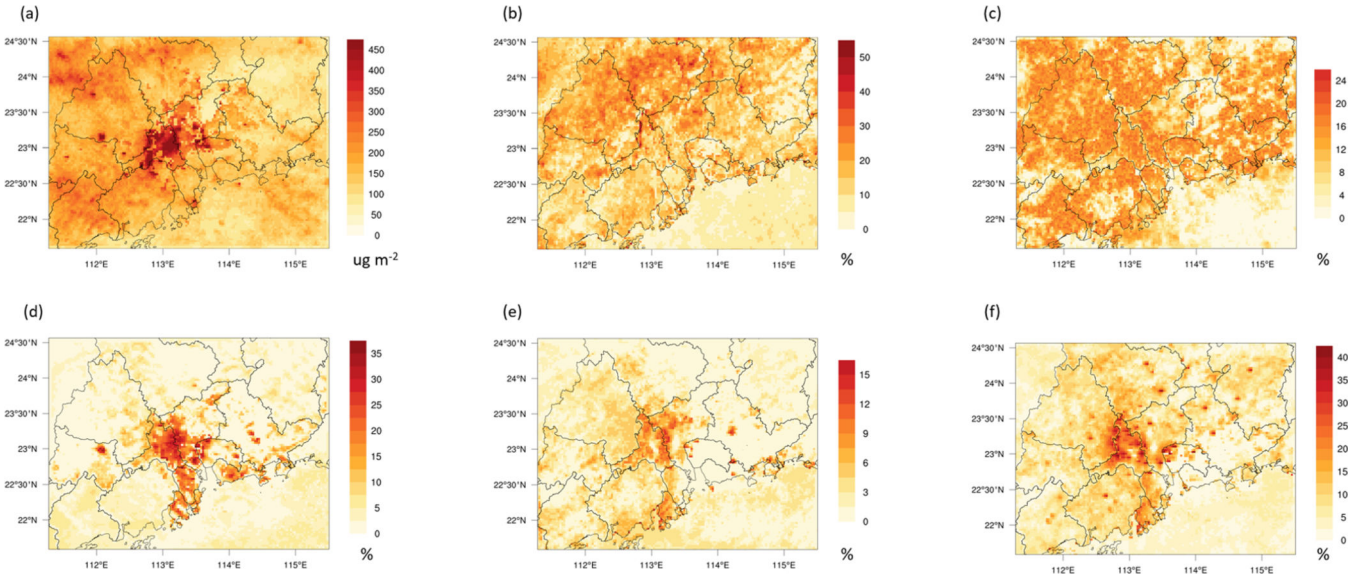

Fig. 7.

(a) Model-predicted THg deposition ($\mu g \cdot m^{-2} \cdot yr^{-1}$), Difference of THg deposition between the (b) BCs, (c) NAT, (d) PP, (e) MSWI, (f) IP scenario and BASE scenario (%)

Table 1

Emission factors and Hg speciation of anthropogenic sources.

Source category	Emission factor ($g.t^{-1}$)	Hg speciation (%)		
		GEM	GOM	PBM
1 Power plant	0.05[a]	71[a]	27	2
2 Municipal solid wastes incineration	0.21[b]	19[b]	79	2
3 Industrial point sources	-			
Industrial boilers	0.10[a]	60[a]	37	3
Iron and steel production	0.04[c]	34[c]	65	1
Cement production	0.14[a]	49[a]	50	1
Non-ferrous metals production (Zn, Cu, Pb)	-			
Zn smelting	3.60[a]	46[a]	49	5
Cu smelting	0[a]	46[a]	49	5
Pb smelting	1.70[a]	46[a]	49	5
4 Non-industrial anthropogenic sources	-			
On-road mobile sources	0.01[a]	50[a]	40	10
Residential boilers	0.14[a]	72[a]	8	20
Biomass incineration	0.01[a]	72[a]	8	20

[a] From Wu et al. (2016)

[b] From Chen et al. (2013)

[c] From Zhang et al. (2015)

Table 2

Mercury emission inventory in PRD for 2014

Sources	Emission (kg)	GEM (kg)	Hg speciation GOM (kg)	PBM (kg)
1 Power plants	3510.2	2492.2	947.8	70.2
2 Municipal solid wastes incineration	578.3	109.9	451.1	17.4
3 Industrial point sources	7825.4	3917.6	3653.1	254.7
Industrial boilers	2710.7	1626.4	1003.0	81.3
Iron and steel production	1396.3	474.7	907.6	14.0
Cement production	2649.9	1325.0	1219.0	106.0
Non-ferrous metals production (Zn, Cu, Pb)	1068.5	491.5	523.6	53.4
Zn smelting	880.8	405.2	431.6	44.0
Cu smelting	0.0	0.0	0.0	0.0
Pb smelting	187.7	86.3	92.0	9.4
4 Non-industrial anthropogenic sources	25.7	14.9	7.2	3.5
On-road mobile	16.2	8.1	6.5	1.6
Residential boilers	5.1	3.7	0.4	1.0
Biomass incineration	4.4	3.2	0.4	0.9
Total mercury emission	11939.6	6534.7(55.0%)	5059.1(42.0%)	345.8(3.0%)

Table 3

Validation of meteorology results (January, April, July and October in 2014)

Station	Parameters		avg	N*	Bias	NME	NMB	R	IOA
Sugang	Relative Humidity (%)	Obs	60.5	2917	9.7	18.1	16.1	0.84	0.83
		Model	70.2						
	Temperature (℃)	Obs	24.2	2916	−0.9	7.1	−3.8	0.95	0.97
		Model	23.3						
	Wind Speed (m/s)	Obs	1.0	2911	1.3	138.0	132.0	0.55	0.50
		Model	2.4						
Yuanling	Relative Humidity(%)	Obs	56.7	2761	12.9	23.5	22.9	0.84	0.80
		Model	69.6						
	Temperature (℃)	Obs	25.2	2789	−1.6	8.9	−6.3	0.94	0.95
		Model	23.6						
	Wind Speed (m/s)	Obs	1.5	2789	0.5	50.5	29.9	0.55	0.66
		Model	2.0						

Table 4

Comparisons of model results in BASE scenario with observations

Station	Sampling period	Observation TGM/GEM ($ng \cdot m^{-3}$)	Model TGM/GEM ($ng \cdot m^{-3}$)	Relative bias	Reference
Wangqingsha, Guangdong	Dec-08	2.9	3.20	10.3%	(Wang et al., 2014)
Guangzhou, rural site	Nov-08-Dec-08	2.94	3.42	16.3%	(Lin et al., 2010)
Mt.Dinghu, Guangdong	Oct-09-Apr-10	5.0±2.89	3.84	−24.2%	(Chen et al., 2013)
Guangzhou, urban site	Nov-10-Nov-11	4.6±1.36	3.74	−18.5%	(Chen et al., 2013)

Table 5

Comparisons of simulated mercury deposition in BASE scenario with observations

Station	Sampling period	Observation/Simulation			Reference
		Wet deposition (μg m^{-2} yr^{-1})	Rainfall (mm)	Dry deposition (μg m^{-2} yr^{-1})	
Guangzhou urban site	Jan-10-Dec-12	145.8/148.2	1699/2040	58.6/55.2	(Huang et al., 2016)
Dinghushan site	Jan-10-Dec-12	102.4/113.6	1599/2120	54.6/45.6	(Huang et al., 2016)